

# Quantum interferometric optical lithography: towards arbitrary two-dimensional patterns

Pieter Kok<sup>\*1</sup>, Agedi N. Boto<sup>2</sup>, Daniel S. Abrams<sup>2</sup>, Colin P. Williams<sup>2</sup>, Samuel L. Braunstein<sup>1</sup>  
and Jonathan P. Dowling<sup>2</sup>

<sup>1</sup>*Informatics, Bangor University, Bangor LL57 1UT, UK*

<sup>2</sup>*Jet Propulsion Laboratory, California Institute of Technology,  
Mail Stop 126-347, 4800 Oak Grove Drive, Pasadena, California 91109*

As demonstrated by Boto *et al.* [Phys. Rev. Lett. **85**, 2733 (2000)], quantum lithography offers an increase in resolution below the diffraction limit. Here, we generalize this procedure in order to create patterns in one and two dimensions. This renders quantum lithography a potentially useful tool in nanotechnology.

PACS numbers: 42.50.Hz, 42.25.Hz, 42.65.-k, 85.40.Hp

Optical lithography is a widely used printing method. In this process light is used to etch a substrate. The exposed or unexposed areas on the substrate then define the pattern. In particular, the micro-chip industry uses lithography to produce smaller and smaller processors. However, classical optical lithography can only achieve a resolution comparable to the wavelength of the light used [1–3]. It therefore minimizes the scale of the patterns. To create smaller patterns we need to venture beyond this classical boundary [4]. In Ref. [5] we introduced a procedure called *quantum* lithography that offers an increase in resolution beyond the diffraction limit. This process allows us to write closely spaced lines in one dimension. However, for practical purposes (e.g., optical surface etching) we need to create more complicated patterns in both one and two dimensions. Here, we study how quantum lithography can be extended to create these patterns.

This paper is organized as follows: first, for completeness, we present a derivation of the Rayleigh diffraction limit. Then, in Sec. II we reiterate the method introduced in Ref. [5]. Then, in Sec. III we give a generalized version of the states used in this procedure. We show how we can tailor arbitrary one-dimensional patterns with these states. In Sec. IV we show how four-mode entangled states lead to patterns in two dimensions. Sec. V addresses the physical implementation of quantum lithography.

## I. CLASSICAL RESOLUTION LIMIT

When we talk about optical resolution, we can mean two things: it may denote the minimum distance between two nearby points which can still be resolved with microscopy. Or it can denote the minimum distance separating two points which are printed using lithography. In the limit of geometric optics these resolutions would be identical. In this section we derive the classical resolution limit for interferometric lithography using the so-called Rayleigh criterion [6].

Suppose two plane waves characterised by  $\vec{k}_1$  and  $\vec{k}_2$  hit a surface under an angle  $\theta$  from the normal vector. The wave vectors are given by

$$\vec{k}_1 = k(\cos \theta, \sin \theta) \quad \text{and} \quad \vec{k}_2 = k(\cos \theta, -\sin \theta), \quad (1)$$

where we used  $|\vec{k}_1| = |\vec{k}_2| = k$ . The wave number  $k$  is related to the wavelength of the light according to  $k = 2\pi/\lambda$ .

In order to find the interference pattern in the intensity  $I$ , we sum the two plane waves at position  $\vec{r}$  at the amplitude level:

$$I(\vec{r}) \propto \left| e^{i\vec{k}_1 \cdot \vec{r}} + e^{i\vec{k}_2 \cdot \vec{r}} \right|^2 = 4 \cos^2 \left[ \frac{1}{2} (\vec{k}_1 - \vec{k}_2) \cdot \vec{r} \right]. \quad (2)$$

When we calculate the inner product  $(\vec{k}_1 - \vec{k}_2) \cdot \vec{r}/2$  from Eq. (1) we obtain the expression

$$I(x) \propto \cos^2(kx \sin \theta) \quad (3)$$

for the intensity along the substrate in direction  $x$ .

The Rayleigh criterion states that the minimal resolvable feature size  $\Delta x$  corresponds to the distance between an intensity maximum and an adjacent minimum. From Eq. (3) we obtain

$$k\Delta x \sin \theta = \frac{\pi}{2}. \quad (4)$$

This means that the maximum resolution is given by

$$\Delta x = \frac{\pi}{2k \sin \theta} = \frac{\pi}{2 \left( \frac{2\pi}{\lambda} \sin \theta \right)} = \frac{\lambda}{4 \sin \theta}, \quad (5)$$

where  $\lambda$  is the wavelength of the light. The maximum resolution is therefore proportional to the wavelength and inversely proportional to the sine of the angle between the incoming plane waves and the normal. The resolution is thus maximal ( $\Delta x$  is minimal) when  $\sin \theta = 1$ , or  $\theta = \pi/2$ . This is the grazing limit. The classical diffraction limit is therefore  $\Delta x = \lambda/4$ . Note that this derivation does not use the approximation  $\sin \theta \simeq \theta$ , which is common when considering diffraction phenomena.

## II. INTRODUCTION TO QUANTUM LITHOGRAPHY

In this section we briefly reiterate our method of Ref. [5]. It exploits the physical properties of multi-photon absorption of a substrate. Suppose we have two intersecting light beams  $a$  and  $b$ . We place a substrate sensitive to  $N$ -photon absorption at the position where the two beams meet, such that the interference pattern is recorded. For simplicity, we consider the grazing limit in which the angle  $\theta$  off axis for the two beams is  $\pi/2$  (see Fig. II). Classically, the interference pattern on the substrate has a resolution of the order of  $\lambda/4$ , where  $\lambda$  is the wavelength of the light. However, by using entangled photon-number states (i.e., inherently *non-classical* states) we can increase the resolution well into the sub-wavelength regime.

How does quantum lithography work? Let the two counter-propagating light beams  $a$  and  $b$  be in the combined entangled state of  $N$  photons

$$|\psi_N\rangle_{ab} = (|N, 0\rangle_{ab} + e^{iN\varphi}|0, N\rangle_{ab})/\sqrt{2}, \quad (6)$$

where  $\varphi = kx/2$ , with  $k = 2\pi/\lambda$ . We define the mode operator  $\hat{e} = (\hat{a} + \hat{b})/\sqrt{2}$  and its adjoint  $\hat{e}^\dagger = (\hat{a}^\dagger + \hat{b}^\dagger)/\sqrt{2}$ . The deposition rate  $\Delta$  on the substrate is then given by

$$\Delta_N = \langle \psi_N | \hat{\delta}_N | \psi_N \rangle \quad \text{with} \quad \hat{\delta}_N = \frac{(\hat{e}^\dagger)^N \hat{e}^N}{N!}, \quad (7)$$

i.e., we look at the higher moments of the electric field operator [7–9]. The deposition rate  $\Delta$  is measured in units of intensity. Leaving the substrate exposed for a time  $t$  to the light source will result in an exposure pattern  $P(\varphi) = \Delta_N t$ . After a straightforward calculation we see that

$$\Delta_N \propto (1 + \cos N\varphi). \quad (8)$$

We interpret this as follows. A path-differential phase-shift  $\varphi$  in light beam  $b$  results in a displacement  $x$  of the interference pattern on the substrate. Using two classical waves, a phase-shift of  $2\pi$  will return the pattern to its original position. However, according to Eq. (8), one cycle is completed after a shift of  $2\pi/N$ . This means that a shift of  $2\pi$  will displace the pattern  $N$  times. In other words, we have  $N$  times more maxima in the interference pattern. These need to be closely spaced, yielding an effective Rayleigh resolution of  $\Delta x = \lambda/4N$ , a factor of  $N$  below the classical interferometric result of  $\Delta x = \lambda/4$  [1].

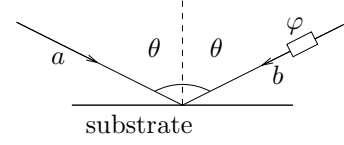


Fig. 1. Two light beams  $a$  and  $b$  cross each other at the surface of a photosensitive substrate. The angle between them is  $2\theta$  and they have a relative phase difference  $\varphi = kx/2$ . We consider the limit case of  $\theta \rightarrow \pi/2$ .

Physically, we can interpret this result as follows: instead of having a state of  $N$  single photons, Eq. (6) describes an  $N$ -photon state. Since the momentum of this state is  $N$  times as large as the momentum for a single photon, the corresponding DeBroglie wavelength is  $N$  times smaller. The interference of this  $N$ -photon state with itself on a substrate thus gives a periodic pattern with a characteristic resolution dimension of  $\Delta x = \lambda/4N$ .

## III. GENERAL PATTERNS IN 1D

So far, we have described a method to print a simple pattern of evenly spaced lines of sub-wavelength resolution. However, for any practical application we need the ability to produce more complicated patterns. To this end, we introduce the state

$$|\psi_{Nm}\rangle_{ab} = \left( e^{im\varphi} |N - m, m\rangle_{ab} + e^{i(N-m)\varphi} e^{i\theta_m} |m, N - m\rangle_{ab} \right) / \sqrt{2}. \quad (9)$$

This is a generalized version of Eq. (6). In particular, Eq. (9) reduces to Eq. (6) when  $m = 0$  and  $\theta_m = 0$ . Note that we included a relative phase  $e^{i\theta_m}$ , which will turn out to be crucial in the creation of arbitrary one-dimensional patterns.

We can calculate the deposition rate again according to the procedure in Sec. II. As we shall see later, in general, we can have superpositions of the states given by Eq. (9). We therefore have to take into account the possibility of different values of  $m$ , yielding a quantity

$$\Delta_{Nm}^{Nm'} = \langle \psi_{Nm} | \hat{\delta}_N | \psi_{Nm'} \rangle. \quad (10)$$

Note that this deposition rate depends not only on the parameter  $\varphi$ , but also on the relative phases  $\theta_m$  and  $\theta_{m'}$ . The deposition rate then becomes

$$\Delta_{Nm}^{Nm'} \propto \sqrt{\binom{N}{m} \binom{N}{m'}} \left[ e^{i(m'-m)\varphi} + e^{i(N-m-m')\varphi} e^{i\theta_{m'}} + e^{-i(N-m-m')\varphi} e^{-i\theta_m} + e^{-i(m'-m)\varphi} e^{i(\theta_{m'} - \theta_m)} \right], \quad (11)$$

where  $\binom{N}{m}$  means  $N!/(N-m)!m!$ . Obviously,  $\langle \psi_{Nm} | \hat{\delta}_l | \psi_{N'm'} \rangle = 0$  when  $l \notin \{N, N'\}$ . For  $m = m'$ , the deposition rate takes on the form

$$\Delta_{Nm} \propto \binom{N}{m} \{1 + \cos[(N-2m)\varphi + \theta_m]\}, \quad (12)$$

which, in the case of  $m = 0$  and  $\theta_m = 0$ , coincides with Eq. (8). When  $\theta_m$  is suitably chosen, we see that we also have access to deposition rates  $(1 - \cos N\varphi)$  and  $(1 \pm \sin N\varphi)$ . Apart from this extra phase freedom, Eq. (12) does not look like an improvement over Eq. (8), since  $N - 2m \leq N$ , which means that the resolution decreases. However, we will show later how these states *can* be used to produce non-trivial patterns.

First, we look at a few special cases of  $\theta_m$  and  $\theta_{m'}$ . When we write  $\Delta_{Nm'}^{Nm'} = \Delta_{Nm'}^{Nm'}(\theta_m, \theta_{m'})$  we have

$$\Delta_{nm'}^{Nm'}(0, 0) \propto \cos\left(\frac{N-2m}{2}\varphi\right) \cos\left(\frac{N-2m'}{2}\varphi\right), \quad (13a)$$

$$\Delta_{Nm'}^{Nm'}(0, \pi) \propto \cos\left(\frac{N-2m}{2}\varphi\right) \sin\left(\frac{N-2m'}{2}\varphi\right), \quad (13b)$$

$$\Delta_{Nm'}^{Nm'}(\pi, 0) \propto \sin\left(\frac{N-2m}{2}\varphi\right) \cos\left(\frac{N-2m'}{2}\varphi\right), \quad (13c)$$

$$\Delta_{Nm'}^{Nm'}(\pi, \pi) \propto \sin\left(\frac{N-2m}{2}\varphi\right) \sin\left(\frac{N-2m'}{2}\varphi\right). \quad (13d)$$

These relations give the dependence of the matrix elements  $\Delta_{Nm'}^{Nm'}$  on  $\theta_m$  and  $\theta_{m'}$  in a more intuitive way than Eq. (11) does. Finally, when  $\theta_m = \theta_{m'} = \theta$  we obtain

$$\Delta_{Nm'}^{Nm'} \propto \cos\left[\frac{(N-2m)\varphi + \theta}{2}\right] \cos\left[\frac{(N-2m')\varphi - \theta}{2}\right]. \quad (14)$$

So far we have only considered generalized deposition rates given by Eq. (9), with special values of their parameters. We will now turn our attention to the problem of creating more arbitrary patterns.

Note that there are two main, though fundamentally different, ways we can superpose the states given by Eq. (9). We can superpose states with different photon numbers  $n$  and a fixed distribution  $m$  over the two modes:

$$|\Psi_m\rangle = \sum_{n=0}^N \alpha_n |\psi_{nm}\rangle, \quad (15)$$

with  $\alpha_n$  complex coefficients. This is a superposition of states with *different* total photon number in each branch. Alternatively, we can superpose states with a fixed photon number  $N$ , but with different distributions  $m$ :

$$|\Psi_N\rangle = \sum_{m=0}^{\lfloor N/2 \rfloor} \alpha_m |\psi_{Nm}\rangle, \quad (16)$$

where  $\lfloor N/2 \rfloor$  denotes the largest integer  $l$  with  $l \leq N/2$  and  $\alpha_m$  again the complex coefficients. Every branch in this superposition is an  $N$ -photon state.

These two different superpositions can be used to tailor patterns which are more complicated than just closely spaced lines. We will now study these two different methods.

## A. The Pseudo-Fourier Method

The first method, corresponding to the superposition given by Eq. (15), we will call the pseudo-Fourier method (this choice of name will become clear shortly). When we calculate the deposition rate  $\Delta_m$  according to the state  $|\Psi_m\rangle$  we immediately see that branches with different photon numbers  $n$  and  $n'$  do not exhibit interference:

$$\Delta_m = \sum_{n=0}^N |\alpha_n|^2 \langle \psi_{nm} | \hat{\delta}_n | \psi_{nm} \rangle = \sum_{n=0}^N |\alpha_n|^2 \Delta_{nm}. \quad (17)$$

Using Eq. (12) the exposure pattern  $P(\varphi) = \Delta_m t$  becomes

$$P(\varphi) = t \sum_{n=0}^N c_n \{1 + \cos[(n-2m)\varphi + \theta_n]\}, \quad (18)$$

where  $t$  is the exposure time and the  $c_n$  are real and positive. Since  $m < n$  and  $m$  is fixed, we have  $m = 0$ . We will now prove that this is a Fourier series up to a constant.

A general Fourier expansion of  $p(\varphi)$  can be written as

$$P(\varphi) = \sum_{n=0}^N (a_n \cos n\varphi + b_n \sin n\varphi). \quad (19)$$

Writing Eq. (18) as

$$P(\varphi) = t \sum_{n=0}^N c_n + t \sum_{n=0}^N c_n \cos(n\varphi + \theta_n), \quad (20)$$

where  $t \sum_{n=0}^N c_n$  is a constant. If we ignore this constant (its contribution to the deposition rate will give a general uniform background exposure of the substrate, since it is independent of  $\varphi$ ) we see that we need

$$c_n \cos(n\varphi + \theta_n) = a_n \cos n\varphi + b_n \sin n\varphi \quad (21)$$

with  $c_n$  positive,  $\theta_n \in [0, 2\pi)$  and  $a_n, b_n$  real. Expanding the left-hand side and equating terms in  $\cos n\varphi$  and  $\sin n\varphi$  we find

$$a_n = c_n \cos \theta_n \quad \text{and} \quad b_n = c_n \sin \theta_n. \quad (22)$$

This is essentially a co-ordinate change from Cartesian to polar co-ordinates. Thus, Eq. (18) is equivalent to a Fourier series up to an additive constant. Since in the limit of  $N \rightarrow \infty$  a Fourier series can converge to any well-behaved pattern  $P(\varphi)$ , this procedure allows us to approximate arbitrary patterns in one dimension (up to a constant). It is now clear why we call this procedure the pseudo-Fourier method.

However, there is a drawback with this procedure. The deposition rate  $\Delta$  is a positive definite quantity, which means that once the substrate is exposed at a particular Fourier component, there is no way this can be undone. Technically, Eq. (18) can be written as

$$P(\varphi) = Q \cdot t + t \sum_{n=0}^N (a_n \cos n\varphi + b_n \sin n\varphi), \quad (23)$$

where  $Q$  is the uniform background ‘penalty exposure rate’  $Q = \sum_{n=0}^N c_n$  we mentioned earlier. The second term on the right-hand side is a true Fourier series. Thus in the pseudo-Fourier method there is always a minimum exposure of the substrate. Ultimately, this penalty can be traced to the absence of interference between the terms with different photon number in Eq. (15). Next, we will investigate whether our second method of tailoring patterns can remove this penalty exposure.

## B. The Superposition Method

We will now study our second method of tailoring patterns, which we call the ‘superposition method’ (lacking a better name). Here we keep the total number of photons  $N$  constant, and change how the photons are distributed between the two beams in each branch [see Eq. (16)]. A distinct advantage of this method is that it *does* exhibit interference between the different branches in the superposition, which eliminates the uniform background penalty exposure.

Take for instance a superposition of two distinct terms

$$|\Psi_N\rangle = \alpha_m |\psi_{Nm}\rangle + \alpha_{m'} |\psi_{Nm'}\rangle, \quad (24)$$

with  $|\alpha_m|^2 + |\alpha_{m'}|^2 = 1$  and  $|\psi_{nm}\rangle$  given by Eq. (11). After some algebraic manipulation the deposition rate can be written as

$$\begin{aligned} \Delta_N \propto & |\alpha_m|^2 \binom{N}{m} \{1 + \cos[(N - 2m)\varphi + \theta_m]\} \\ & + |\alpha_{m'}|^2 \binom{N}{m'} \{1 + \cos[(N - 2m')\varphi + \theta_{m'}]\} \\ & + 8r_m^{m'} \sqrt{\binom{N}{m} \binom{N}{m'}} \cos\left(\frac{\theta_{m'}}{2} - \frac{\theta_m}{2} + \xi_m^{m'}\right) \\ & \times \cos\frac{1}{2}[(N - 2m)\varphi + \theta_m] \\ & \times \cos\frac{1}{2}[(N - 2m')\varphi + \theta_{m'}], \end{aligned} \quad (25)$$

where the deposition rate  $\Delta$  is now a function of  $\alpha_m$  and  $\alpha_{m'}$ , where we have chosen the real numbers  $r_m^{m'}$  and  $\xi_m^{m'}$  to satisfy  $\alpha_m^* \alpha_{m'} \equiv r_m^{m'} \exp(i\xi_m^{m'})$ . For the special values  $N = 20$ ,  $m = 9$ ,  $m' = 5$  and  $\theta_m = \theta_{m'} = 0$  we obtain the pattern shown in Fig. IV. Clearly, there is no uniform background penalty exposure here.

$\Delta_{20}$ , with  $m = 5$  and  $m' = 9$ .

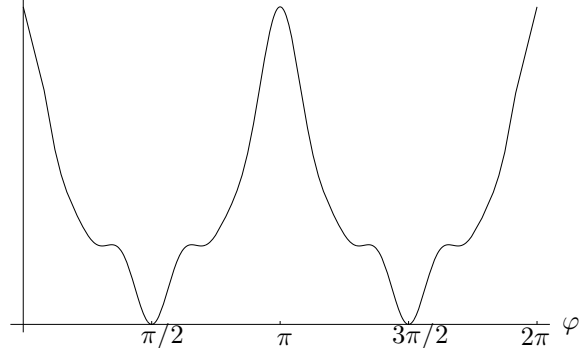


Fig. 2: The deposition rate due to a superposition of two states containing 20 photons with distributions  $m = 9$  and  $m' = 5$  ( $\theta_m = \theta_{m'} = 0$ ). The deposition rate at  $\varphi = \pi/2$  and  $\varphi = 3\pi/2$  is zero, which means that there is no general uniform background exposure.

For more than two branches in the superposition this becomes a complicated function, which is not nearly as well understood as a Fourier series. The general expression for the deposition rate can be written as

$$\begin{aligned} \Delta_N \propto & \sum_{m=0}^{\lfloor N/2 \rfloor} \sum_{m'=0}^{\lfloor N/2 \rfloor} r_m^{m'} \sqrt{\binom{N}{m} \binom{N}{m'}} \\ & \times \cos\left(\frac{\theta_{m'}}{2} - \frac{\theta_m}{2} + \xi_m^{m'}\right) \\ & \times \cos\frac{1}{2}[(N - 2m)\varphi + \theta_m] \\ & \times \cos\frac{1}{2}[(N - 2m')\varphi + \theta_{m'}], \end{aligned} \quad (26)$$

where we have chosen  $r_m^{m'}$  and  $\xi_m^{m'}$  real to satisfy  $\alpha_m^* \alpha_{m'} \equiv r_m^{m'} \exp(i\xi_m^{m'})$ . Note that  $\xi_m^m = 0$ .

If we want to tailor a pattern  $F(\varphi)$ , it might be the case that this type of superposition will also converge to the required pattern. We will now compare the superposition method with the Fourier method.

## C. Comparing the two methods

So far, we discussed two methods of creating non-trivial patterns in one dimension. The Fourier method

is simple but yields a uniform background penalty exposure. The superposition method is far more complicated, but seems to get around the background exposure. Before we make a comparison between the two methods we will discuss the creation of ‘arbitrary’ patterns.

It is well known that any sufficiently well-behaved periodic function can be written as an infinite Fourier series (we ignore such subtleties which arise when two functions differ only at a finite number of points, etc.). However, when we create patterns with the pseudo-Fourier lithography method we do not have access to every component of the Fourier expansion, since this would involve an infinite number of photons ( $n \rightarrow \infty$ ). This means that we can only employ truncated Fourier series, and these can merely approximate arbitrary patterns.

The Fourier expansion has the nice property that when a series is truncated at  $N$ , the remaining terms still give the best Fourier expansion of the function up to  $N$ . In other words, the coefficients of a truncated Fourier series are equal to the first  $N$  coefficients of a full Fourier series. If the full Fourier series is denoted by  $F$  and the truncated series by  $F_N$ , we can define the normed-distance quantity  $D_N$ :

$$D_N \equiv \int_0^{2\pi} |F(\varphi) - F_N(\varphi)|^2 d\varphi, \quad (27)$$

which can be interpreted as a distance between  $F$  and  $F_N$ . If quantum lithography yields a pattern  $p_N(\varphi) = \Delta_N t$ , we can introduce the following definition: quantum lithography can approximate arbitrary patterns if

$$\int_0^{2\pi} |F(\varphi) - P_N(\varphi)|^2 d\varphi \leq \varepsilon D_N, \quad (28)$$

with  $\varepsilon$  some real, positive definite proportionality constant. This definition gives the concept of approximating patterns a solid basis.

We compare the Fourier and the superposition method for one special case. We choose the test function

$$F(\varphi) = \begin{cases} h & \text{if } -\frac{\pi}{2} < \varphi < \frac{\pi}{2}, \\ 0 & \text{otherwise.} \end{cases} \quad (29)$$

With up to ten photons, we ask how well the Fourier and the superposition method approximate this pattern.

In the case of the Fourier method the solution is immediate. The Fourier expansion of the ‘trench’ function given by Eq. (29) is well known:

$$F(\varphi) = \sum_{q=0}^{\infty} \frac{(-1)^q}{2q+1} \cos[(2q+1)\varphi]. \quad (30)$$

Using up to  $n = 10$  photons we include terms up to  $q = 4$ , since  $2q+1 \leq 10$ . The Fourier method thus yields a pattern  $P(\varphi)$  (the two patterns  $P(\varphi)$  and  $F(\varphi)$  are generally

not the same) which can be written as

$$P(\varphi) = \sum_{q=0}^4 \frac{c_q t}{2q+1} (1 + \cos[(2q+1)\varphi + \pi\kappa_q]), \quad (31)$$

where  $c_q$  is a constant depending on the proportionality constant of  $\Delta_{2q+1}$ , the rate of production of  $|\psi_{nm}\rangle$  and the coupling between the light field and the substrate. The term  $\kappa_q$  is defined to accommodate for the minus signs in Eq. (30): it is zero when  $q$  is even and one when  $q$  is odd. Note the uniform background penalty exposure rate  $\sum_{q=0}^4 c_q/(2q+1)$ . The result of this method is shown in Fig. IV.

Alternatively, the superposition method employs a state

$$|\Psi_N\rangle = \sum_{m=0}^{\lfloor N/2 \rfloor} \alpha_m |\psi_{Nm}\rangle. \quad (32)$$

The procedure of finding the best fit with the test function is more complicated. We have to minimize the absolute difference between the deposition rate  $\Delta_N(\vec{\alpha})$  times the exposure time  $t$  and the test function  $F(\varphi)$ . We have chosen  $\vec{\alpha} = (\alpha_0, \dots, \alpha_{n/2})$ . Mathematically, we have to evaluate the  $\vec{\alpha}$  and  $t$  which minimize  $d_N$ :

$$d_N = \int_0^{2\pi} |F(\varphi) - \Delta_N(\vec{\alpha})t|^2 d\varphi,$$

with

$$\Delta_N(\vec{\alpha}) = \langle \Psi_N | \hat{\delta}_N | \Psi_N \rangle. \quad (33)$$

We have to fit both  $t$  and  $\vec{\alpha}$ . Using a genetic optimization algorithm [10] (with  $h = 1$ , a normalized height of the test function) we found that the deposition rate is actually very close to zero in the interval  $\pi/2 \leq \varphi \leq 3\pi/2$ , unlike the pseudo-Fourier method, where we have to pay a uniform background penalty. This result implies that in this case a superposition of different photon distributions  $m$ , given a fixed total number of photons  $N$ , works better than a superposition of different photon number states (see Fig. IV). In particular, *the fixed photon number method allows for the substrate to remain virtually unexposed in certain areas.*

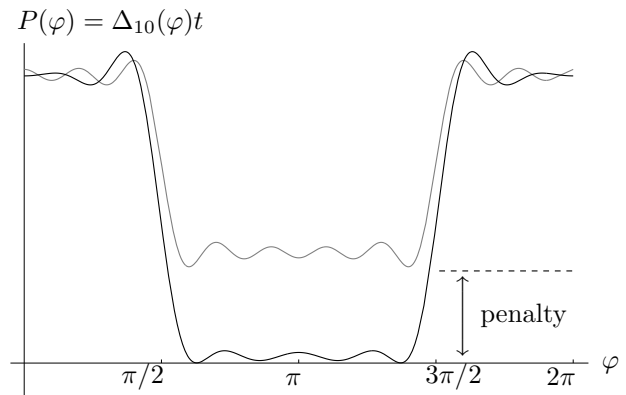


Fig. 3: The deposition rate on the substrate resulting from a superposition of states with  $N = 10$  and different  $m$  (black curve), and also resulting from a superposition of states with different  $n$  with  $m = 0$  (grey curve). The coefficients of the superposition that yield the black curve are optimized using a genetic algorithm [10], while the grey curve is a truncated pseudo-Fourier series. Notice the ‘penalty’ (displacement from zero) of the deposition rate for the pseudo-Fourier series between  $\pi/2$  and  $3\pi/2$ .

We stress that this is merely a comparison for a specific example, namely that of the trench target function  $F(\varphi)$ . We conjecture that the superposition method can approximate other arbitrary patterns equally well, but we have not yet found a proof. Besides the ability to fit an arbitrary pattern, another criterion of comparison between the pseudo-Fourier method and the superposition method, is the time needed to create the  $N$ -photon entangled states.

Until now, we have only considered sub-wavelength resolution in one direction, namely parallel to the direction of the beams. However, for practical applications we would like sub-wavelength resolution in both directions on the substrate. This is the subject of the next section.

#### IV. GENERAL PATTERNS IN 2D

In this section we study how to create two-dimensional patterns on a suitable substrate using the quantum lithography techniques developed in the previous sections. As we have seen, the phase shift  $\varphi$ , in the setup given by Fig. II, acts as a parametrization for the deposition rate in one dimension. Let’s call this the  $x$ -direction.

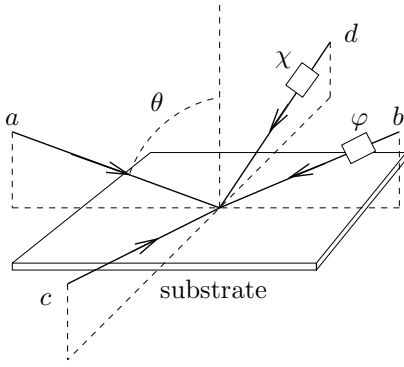


Fig. 4: Four light beams  $a$ ,  $b$ ,  $c$  and  $d$  cross each other at the surface of a photosensitive substrate. The angles between  $a$  and  $b$  and  $c$  and  $d$  are again taken in the grazing limit of  $\theta = \pi/2$ . The relative phase difference between  $a$  and  $b$  is  $\varphi$  and the relative phase difference between  $c$  and  $d$  is  $\chi$ .

We can now do the same for the  $y$ -direction, employing two counter-propagating beams ( $c$  and  $d$ ) in the  $y$ -direction (see Fig. ). The same conditions apply: we consider the limit where the spatial angle  $\theta$  off axis approaches  $\pi/2$ , thus grazing along the substrate’s surface.

Consider the region where the four beams  $a$ ,  $b$ ,  $c$  and  $d$  overlap. For real lithography we have to take into account the mode shapes, but when we confine ourselves to an area with side lengths  $\lambda$  (where  $\lambda$  is the wavelength of the used light) this problem does not arise.

The class of states on modes  $a$  to  $d$  that we consider here are of the form

$$|\psi_{Nm}^k\rangle = \frac{1}{2} \left[ e^{im\varphi} |N-m, m; 0, 0\rangle + e^{i(N-m)\varphi} e^{i\zeta_m} |m, N-m; 0, 0\rangle + e^{ik\theta} |0, 0; N-k, k\rangle + e^{i(N-k)\chi} e^{i\bar{\zeta}_k} |0, 0; k, N-k\rangle \right], \quad (34)$$

where  $\zeta_m$  and  $\bar{\zeta}_k$  are two relative phases. This is by no means the only class of states, but we will restrict our discussion to this one for now. Observe that this is a superposition on the amplitude level, which allows destructive interference in the deposition rate in order to create dark spots on the substrate. Alternatively, we could have used the one-dimensional method [with states given by Eq. (9)] in the  $x$ - and  $y$ -direction, but this cannot give interference effects between the modes  $a, b$  and  $c, d$ .

The phase-shifts  $\varphi$  and  $\chi$  in the light beams  $b$  and  $d$  (see Fig. ) result in respective displacements  $x$  and  $y$  of the interference pattern on the substrate. A phase-shift of  $2\pi$  in a given direction will displace the pattern, say,  $N$  times. This means that the maxima are closer together, yielding an effective resolution equal to  $\Delta x = \Delta y = \lambda/4N$ . This happens in both the  $x$ - and the  $y$ -direction.

We proceed again as in Sec. II by evaluating the  $N^{\text{th}}$  order moment  $\hat{\delta}_N$  of the electric field operator [see Eq. (7)]. This gives the deposition rate  $\Delta_{Nm k'}^{Nm' k'} = \langle \psi_{Nm}^k | \delta_N | \psi_{Nm'}^{k'} \rangle$  [with  $|\psi_{Nm}^k\rangle$  given by Eq. (34)]:

$$\begin{aligned} \Delta_{Nm k'}^{Nm' k'} \propto & \binom{N}{m} \binom{N}{m'} \left( e^{-im\varphi} e^{im'\varphi} + e^{-im\varphi} e^{i(N-m)\varphi} e^{i\zeta_m'} + e^{-i(N-m)\varphi} e^{im'\varphi} e^{-i\zeta_m} \right. \\ & \left. + e^{-i(N-m)\varphi} e^{i(N-m')\varphi} e^{-i(\zeta_m - \zeta_m')} \right) \\ & + \binom{N}{m} \binom{N}{k'} \left( e^{-im\varphi} e^{ik'\chi} + e^{-im\varphi} e^{i(N-k)\chi} e^{i\bar{\zeta}_k'} + e^{-i(N-m)\varphi} e^{ik'\chi} e^{-i\zeta_m} \right) \end{aligned}$$

$$\begin{aligned}
& + e^{-i(N-m)\varphi} e^{i(N-k')\chi} e^{-i(\zeta_m - \bar{\zeta}_{k'})} \Big) \\
& + \binom{N}{k} \binom{N}{m'} \left( e^{-ik\chi} e^{im'\varphi} + e^{-ik\chi} e^{i(N-m')\varphi} e^{i\zeta_{m'}} + e^{-i(N-k)\chi} e^{im'\varphi} e^{-i\bar{\zeta}_k} \right. \\
& \quad \left. + e^{-i(N-k)\chi} e^{i(N-m')\varphi} e^{-i(\bar{\zeta}_k - \zeta_{m'})} \right) \\
& + \binom{N}{k} \binom{N}{k'} \left( e^{-ik\chi} e^{ik'\chi} + e^{-ik\chi} e^{i(N-k')\chi} e^{i\bar{\zeta}_{k'}} + e^{-i(N-k)\chi} e^{ik'\chi} e^{-i\bar{\zeta}_k} \right. \\
& \quad \left. + e^{-i(N-k)\chi} e^{i(N-k')\chi} e^{-i(\bar{\zeta}_k - \bar{\zeta}_{k'})} \right) . \tag{35}
\end{aligned}$$

For the special choice of  $m' = m$  and  $k' = k$  we have

$$\begin{aligned}
\Delta_{Nm}^k & \propto \binom{N}{m}^2 (1 + \cos[(N-2m)\varphi + \zeta_m]) + \binom{N}{k}^2 (1 + \cos[(N-2k)\chi + \bar{\zeta}_k]) \\
& + 4 \binom{N}{m} \binom{N}{k} \cos \frac{1}{2} [N(\varphi - \chi) + (\zeta_m - \bar{\zeta}_k)] \\
& \quad \times \cos \frac{1}{2} [(N-2m)\varphi - \zeta_m] \cos \frac{1}{2} [(N-2k)\chi - \bar{\zeta}_k] . \tag{36}
\end{aligned}$$

We can again generalize this method and use superpositions of the states given in Eq. (34). Note that there are now three numbers  $N$ ,  $m$  and  $k$  which can be varied. Furthermore, as we have seen in the one-dimensional case, superpositions of different  $n$  do not give interference terms in the deposition rate.

Suppose we want to approximate a pattern  $F(\varphi, \chi)$ , with  $\{\varphi, \chi\} \in [0, 2\pi]$ . This pattern can always be written in a Fourier expansion:

$$\begin{aligned}
F(\varphi, \chi) & = \sum_{p,q=0}^{\infty} a_{pq} \cos p\varphi \cos q\chi + b_{pq} \cos p\varphi \sin q\chi \times \\
& \quad c_{pq} \sin p\varphi \cos q\chi + d_{pq} \sin p\varphi \sin q\chi . \tag{37}
\end{aligned}$$

with  $a_{pq}$ ,  $b_{pq}$ ,  $c_{pq}$  and  $d_{pq}$  real. In the previous section we showed that quantum lithography could approximate the Fourier series of a one-dimensional pattern up to a constant displacement. This relied on absence of interference between the terms with different photon numbers. The question is now whether we can do the same for patterns in *two* dimensions. Or alternatively, can general superpositions of the state  $|\psi_{Nm}^k\rangle$  approximate the pattern  $F(\varphi, \chi)$ ?

From Eq. (35) it is not obvious that we can obtain the four trigonometric terms given by the Fourier expansion of Eq. (37):

$$\Delta \propto \cos p\varphi \cos q\chi , \tag{38a}$$

$$\Delta \propto \cos p\varphi \sin q\chi , \tag{38b}$$

$$\Delta \propto \sin p\varphi \cos q\chi , \tag{38c}$$

$$\Delta \propto \sin p\varphi \sin q\chi . \tag{38d}$$

We can therefore not claim that two-dimensional quantum lithography can approximate arbitrary patterns in the sense of one-dimensional lithography. Only simple

patterns like the one given in Fig. can be inferred from Eq. (35). In order to find the best fit to an arbitrary pattern one has to use a minimization procedure.

For example, we calculate the total deposition rate due to the quantum state  $|\Psi_N\rangle$ , where

$$|\Psi_N\rangle = \sum_{m=0}^{\lfloor N/2 \rfloor} \sum_{k=0}^{\lfloor N/2 \rfloor} \alpha_{mk} |\psi_{Nm}^k\rangle . \tag{39}$$

Here,  $\alpha_{mk}$  are complex coefficients. We now proceed by choosing a particular intensity pattern  $F(\varphi, \chi)$  and optimising the coefficients  $\alpha_{mk}$  for a chosen number of photons. The deposition rate due to the state  $|\Psi_N\rangle$  is now

$$\Delta_N(\vec{\alpha}) = \sum_{m,m'=0}^{\lfloor N/2 \rfloor} \sum_{k,k'=0}^{\lfloor N/2 \rfloor} \alpha_{mk}^* \alpha_{m'k'} \Delta_{Nm}^{N'm'k'} , \tag{40}$$

with  $\vec{\alpha} = (\alpha_{0,0}, \alpha_{0,1}, \dots, \alpha_{N/2, N/2})$ . We again have to evaluate the  $\vec{\alpha}$  and  $t$  which minimize

$$\int_0^{2\pi} \int_0^{2\pi} |F(\varphi, \chi) - \Delta_N(\vec{\alpha})t|^2 d\varphi d\chi . \tag{41}$$

The values of  $\vec{\alpha}$  and  $t$  can again be found using a genetic algorithm.

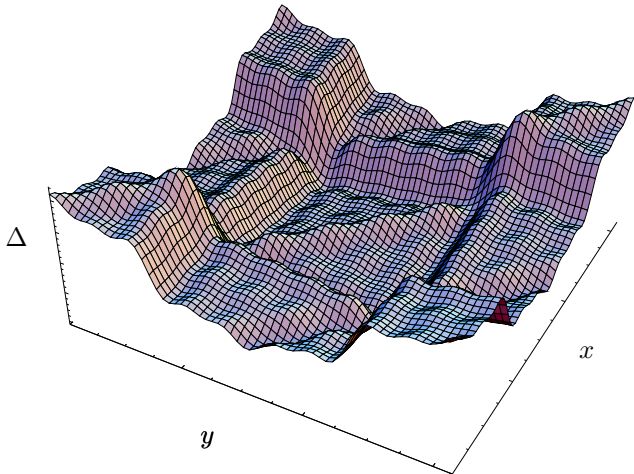


Fig. 5: A simulation of a two-dimensional intensity pattern on an area  $\lambda^2$ , where  $\lambda$  denotes the wavelength of the used light. Here we modelled a square area with sharp edges. The pattern was generated by a Fourier series of up to ten photons (see also Fig. 3 for the one-dimensional case).

## V. PHYSICAL IMPLEMENTATION

With current experimental capabilities, the physical implementation of quantum lithography is very challenging. In particular, there are two major issues to be dealt with before quantum lithography can become a mature technology. First of all, we not only need the ability to create the entangled photon states given by Eqs. (9) and (34), but we should also be able to create coherent superpositions of these states. One possibility might be to use optical components like parametric down-converters. Contrary to the results of Ref. [11], we are not concerned with the usually large vacuum contribution of these processes, since the vacuum will not contribute to the spatial profile of the deposition [see Eqs. (6) and (7)].

Secondly, we need substrates which are sensitive to the higher moments of the electric field operator. When we want to use the pseudo-Fourier method, up to  $N$  photons for quantum lithography in one dimension, the substrate needs to be reasonably sensitive to all the higher moments up to  $N$ , the maximum photon number. Alternatively, we can use the superposition method for  $N$  photons when the substrate is sensitive to predominantly one higher moment corresponding to  $N$  photons. Generally, the method of lithography determines the requirements of the substrate.

There are also some considerations about the approximation of patterns. For example, we might not *need* arbitrary patterns. It might be the case that it is sufficient to have a set of patterns which can then be used to generate any desired circuit. This is analogous to having a universal set of logical gates, permitting any conceivable logical

expression. In that case we only need to determine this elementary set of patterns.

Furthermore, we have to study whether the uniform background penalty exposure really presents a practical problem. One might argue that a sufficient difference between the maximum deposition rate and the uniform background penalty exposure is enough to accommodate lithography. This depends on the details of the substrate's reaction to the electro magnetic field.

Before quantum lithography can be physically implemented and used in the production of nano circuits, these issues have to be addressed satisfactorily.

## VI. CONCLUSIONS

In this paper we have generalized the theory of quantum lithography as first outlined in Ref. [5]. In particular, we have shown how we can create arbitrary patterns in one dimension, albeit with a uniform background penalty exposure. We can also create some patterns in two dimensions, but we have no proof that this method can be extended to give arbitrary patterns.

For lithography in one dimension we distinguish two methods: the pseudo-Fourier method' and the superposition method. The pseudo-Fourier method is conceptually easier since it depends on Fourier analysis, but it also involves a finite amount of unwanted exposure of the substrate. More specifically, the deposition rate equals the pattern in its Fourier basis plus a term yielding unwanted background exposure. The superposition method gets around this problem and seems to give better results, but lacks the intuitive clarity of the Fourier method. Furthermore, we do not have a proof that this method can approximate arbitrary patterns (see Sec. III C for a discussion on this approximation).

Quantum lithography in two dimensions is more involved. Starting with a superposition of states, given by Eq. (34), we found that we can indeed create two-dimensional patterns with sub-wavelength resolution, but we do not have a proof that we can create *arbitrary* patterns. Nevertheless, we might be able to create a certain set of elementary basis patterns.

There are several issues to be addressed in the future. First, we need to study the specific restrictions on the substrate and how we can physically realize them. Secondly, we need to create the various entangled states involved in the quantum lithography protocol.

Finally, G.S. Agarwal and R. Boyd have called to our attention that quantum lithography works also if the weak parametric downconverter source, described in Ref. [5] is replaced by a high-flux optical parametric amplifier [12]. The visibility saturates at 20% in the limit of large gain, but this is quite sufficient for some lithography purposes, as well as for 3D optical holography used for data storage.



## ACKNOWLEDGEMENTS

We would like to acknowledge interesting and useful discussions with G.S. Agarwal, R. Boyd, D. Branning, M. Holland, P.G. Kwiat, Y. Shih, J.E. Sipe, D. Strelakov, R.B. Vrijen and E. Yablonovich. A portion of the research in this paper was carried out at the Jet Propulsion Laboratory, California Institute of Technology, under a contract with the National Aeronautics and Space Administration. In addition, this research was supported by the Office of Naval Research and by project QUICOV under the IST-FET-QIPC programme.

---

\* pieter@sees.bangor.ac.uk

- [1] S.R.J. Brück, *et al.*, *Microelectron. Eng.* **42**, 145 (1998).
- [2] C.A. Mack, *Opt. Phot. News* **7**, 29 (1996).
- [3] M. Mansuripur and R. Liang, *Opt. Phot. News* **11**, 36 (2000).
- [4] E. Yablonovich and R.B. Vrijen, *Opt. Eng.* **38**, 334 (1999).
- [5] A.N. Boto, P. Kok, D.S. Abrams, S.L. Braunstein, C.P. Williams and J.P. Dowling, *Phys. Rev. Lett.* **85**, 2733 (2000).
- [6] Lord Rayleigh, *Phil. Mag.* **8**, 261 (1879).
- [7] M. Göppert-Mayer, *Ann. Phys.* **5**, 273 (1931).
- [8] J. Javanainen and P.L. Gould, *Phys. Rev. A* **41**, 5088 (1990).
- [9] J. Perina Jr., B.E.A. Saleh and M.C. Teich, *Phys. Rev. A* **57**, 3972 (1998).
- [10] K. Price and R. Storn, *Dr. Dobb's Journal*, April, p. 18ff, (1997).
- [11] P. Kok and S.L. Braunstein, *Phys. Rev. A*, to appear.
- [12] G.S. Agarwal and R. Boyd, private communication.